

## Doping the nematic liquid crystal 5CB with milled BaTiO<sub>3</sub> nanoparticles

Alexander Lorenz,<sup>1</sup> Natalie Zimmermann,<sup>1</sup> Satyendra Kumar,<sup>2</sup> Dean R. Evans,<sup>3</sup> Gary Cook,<sup>3,4</sup> and Heinz-S. Kitzerow<sup>1</sup>

<sup>1</sup>*Department of Chemistry, University of Paderborn, Warburger Strasse 100, Paderborn 33098, Germany*

<sup>2</sup>*Department of Physics, Kent State University, Kent, Ohio 44242, USA*

<sup>3</sup>*Air Force Research Laboratory, Materials and Manufacturing Directorate, Wright-Patterson Air Force Base, Ohio 45433, USA*

<sup>4</sup>*Azimuth Corporation, 4134 Linden Avenue, Suite 300, Dayton, Ohio 45432, USA*

(Received 11 July 2012; revised manuscript received 21 September 2012; published 20 November 2012)

The simple nematic mesogen 5CB was doped with milled BaTiO<sub>3</sub> nanoparticles and was investigated with x-ray scattering. Doping with BaTiO<sub>3</sub> nanoparticles of 9 nm in diameter led to the formation of crystallites. These crystallites precipitated and formed a waxlike nanodispersion of 5CB and nanoparticles, which led to intense x-ray scattering signals characteristic of a multilayer structure. Surprisingly, the multilayers possess unusual interlayer spacing, which cannot be explained by simple smectic order of the calamitic molecules.

DOI: [10.1103/PhysRevE.86.051704](https://doi.org/10.1103/PhysRevE.86.051704)

PACS number(s): 61.30.Eb, 61.05.cf, 64.75.Jk

### I. INTRODUCTION

Doping of nematic liquid crystals (LCs) with a small mass fraction of inorganic nanoparticles is of great scientific interest. For example, silica nanoparticles and silica nanoparticles carrying covalently bonded surface functionalization were investigated [1,2]. Recently, the impact of nanoscale particles has been highlighted [3]. For example, a small dopant concentration of surface functionalized nanoparticles can improve the electro-optical performance of LCs or can cause induced dual alignment effects [3,4]. Nanoparticles, surface functionalized with protomesogenic ligands, may even self-assemble into nanoparticulate thermotropic liquid crystalline materials [5,6]. Another approach for surface functionalizing nanoparticles is to use surfactants, such as oleic acid. This method is, in particular, useful to dope LCs with ferroelectric nanoparticles, e.g., BaTiO<sub>3</sub> nanoparticles. For example, ferroelectric nanoparticles coated with a surfactant and dispersed in nematic LCs were reported to enhance the optical diffraction efficiency of beam coupling [7,8], alter the dielectric anisotropy, shift the phase transition temperatures [9,10], and cause asymmetry in the electro-optic response of LCs [11]. Recently, it was reported that dispersions of BaTiO<sub>3</sub> nanoparticles can be prepared by milling cubic BaTiO<sub>3</sub> in heptane with oleic acid in a planetary ball mill [12]. Nanoparticles of 9 nm in average diameter suspended in heptane were obtained by milling for 25 h [12,13]. Stressed BaTiO<sub>3</sub> nanoparticles, which possess permanent electric polarization, can be extracted from such dispersions by harvesting [14].

This paper is focused on x-ray investigations of possible changes in the liquid crystal structure of a simple nematic mesogen caused by doping with inorganic BaTiO<sub>3</sub> nanoparticles. In the present experiments, the well-known nematic LC 4-cyano-4'-pentylbiphenyl (5CB) was doped with milled BaTiO<sub>3</sub> nanoparticles. The LC 5CB shows a nematic phase at ambient temperature and has a clearing temperature of 37 °C. The 5CB molecule has a length of 1.8 nm and forms dimers with a length of 2.5 nm in the isotropic and nematic phases [15,16]. The dimerization is strong in the bulk and may be decreased by surface effects due to polar interactions [17]. The crystalline phase of 5CB also contains dimers [18]. These dimers are stabilized by dipole-dipole interactions between the cyano-biphenyl groups. In the crystal lattice, the 5CB

molecules form a layered structure where each molecular layer possesses one adjacent layer of antiparallel and parallel oriented molecules, respectively. The interlayer distance of two antiparallel oriented layers is only slightly smaller than the interlayer distance between two parallel oriented layers. Thus, the crystal is also characterized by strong London interactions between parallel oriented 5CB molecules. The nanoparticles used for doping were fabricated by milling [12,13], and the resulting heptane dispersion of nanoparticles (9 nm in average diameter) was used for doping without further purification. The doped LC was investigated with both small-angle x-ray scattering (SAXS) and wide-angle x-ray scattering (WAXS). The x-ray scattering signals caused by nanoparticles and by 5CB molecules were detected simultaneously. The investigation reveals that milled BaTiO<sub>3</sub> nanoparticles may cause the growth of crystallites with a multilayered structure of 5CB molecules and may lead to the precipitation into an amorphous material, which can easily be extracted from the LC.

### II. EXPERIMENTAL PROCEDURE

#### A. Preparation of the nanoparticle dispersions and doping

The BaTiO<sub>3</sub> nanoparticles were dispersed in 5CB. First, a dispersion of BaTiO<sub>3</sub> nanoparticles of 9 nm in average diameter was prepared by milling cubic (nonferroelectric) BaTiO<sub>3</sub> for 25 h in a planetary ball mill in the presence of oleic acid as a surfactant and heptane as a solvent [12]. Milling resulted in a dispersion of BaTiO<sub>3</sub> nanoparticles with a concentration of 45 mg/g. It is likely that the stress experienced by cubic BaTiO<sub>3</sub> particles during the milling process converted some of them into tetragonal BaTiO<sub>3</sub>. Consequently, such nanoparticles in the initial dispersion will show ferroelectric properties (i.e., will possess a permanent electric polarization). The initial dispersion of the milled nanoparticles was used without further purification. A doped LC sample was prepared with a concentration of  $c_{\text{doping}} = 5$  mg/g by dissolving 0.028 g of the initial nanoparticle dispersion in 0.25 g of pure 5CB in an open glass vessel and mixing it with a magnetic stirrer. The glass vessel, along with the stirrer, was placed in a fume hood, and the solvent was allowed to slowly evaporate at  $\approx 50$  °C and ambient pressure until the sample mass became constant. The mixture was continuously stirred and was filled in 1.5 mm

diameter quartz Lindemann capillaries. Subsequently, the capillaries were sealed with epoxy and were kept vertically until the phase separation was visually observed.

### B. Small- and wide-angle x-ray scattering

The neat LCs and the nanoparticle dispersion were investigated by x-ray diffraction at the National Synchrotron Light Source (NSLS) beamline X6B. The samples were placed inside a modified Instec (HCS402) hot stage with a temperature precision of  $\pm 0.1$  °C and an *in situ*  $\approx 2.5$  kG magnetic field produced by a pair of CoSm magnets. The capillaries were centered in the x-ray beam, and the temperature was adjusted to 28 °C. A Princeton Instruments CCD camera system (PI-SCX:4300/1-165) with  $2084 \times 2084$  pixels (24 micron pixel, 50 mm chip) and a 2.4:1 fiber ratio option ( $120 \times 120$  mm field of view) was used as the detector. For the first series of experiments, the scattering behavior in the (WAXS) region of  $q = 1.5\text{--}16$  nm $^{-1}$  was studied with an x-ray photon energy of 12 keV and a sample-to-detector distance of 26 cm. Subsequently, the detector was moved to a distance of 120 cm, and the scattering behavior in the region of  $q = 0.3\text{--}3$  nm $^{-1}$  was investigated. Finally, the x-ray photon energy was adjusted to 8 keV, and the scattering was studied in the (SAXS) region of  $q = 0.1\text{--}1.5$  nm $^{-1}$ . Each setup was calibrated with silver behenate [19], and the two-dimensional diffraction patterns were analyzed with MATLAB.

## III. RESULTS

### A. Experiments at a constant temperature of 28 °C

The neat and doped samples were studied at a temperature of 28 °C where the neat 5CB showed a typical diffraction pattern of oriented nematic LCs [Fig. 1(a)]. Nematic LCs show two diffuse peaks in the wide-angle region (only one of them is

shown). The position of these peaks corresponds to the average intermolecular separation in the direction perpendicular to the molecular long axis ( $d_{\perp}$ ) [20]. Additionally, two narrower peaks appear in the small-angle region. The position of the narrow small-angle peaks corresponds to the average intermolecular separation in the direction parallel to the molecular long axis ( $d_{\parallel}$ ) [20]. This characteristic spacing corresponds to the length of the 5CB dimers (2.5 nm) in the nematic phase of 5CB [15]. In contrast to the neat 5CB, the doped sample showed segregation into a phase separated white substance at the bottom of the capillaries. Both the segregated substance and the more transparent upper region were studied separately. No significant difference between the scattering from the upper region of the sample and the scattering from the neat sample could be discerned. In contrast, x-ray diffraction patterns of the white region of the doped LC [Fig. 1(b)] differ considerably from diffraction patterns of the neat LC [Fig. 1(a)]. Diffraction rings appeared in the diffraction patterns of the doped LC because the sample was not oriented by the magnetic field. An intense circular peak appeared in the center of these diffraction patterns [Fig. 1(b)]. Scattering in the wide-angle region also gave rise to a ring in the diffraction patterns rather than an oriented peak. Juxtaposition of the diffraction patterns of the neat and the doped LCs [Fig. 1(c)] shows that the wide-angle reflections in both samples are at approximately the same angle [Fig. 1(c)]. The central peak in the diffraction patterns of the doped LC is surrounded by a ring. This ring and the small-angle scattering caused by the neat compound appear at the same scattering angle. In addition to the scattering patterns recorded at 12 keV, patterns were also recorded at 8 keV as shown in Fig. 1(d) in the small-angle region for the doped LC.

The dependence of scattering intensity on the diffraction angle (or scattering vector, e.g., see Fig. 2) was extracted

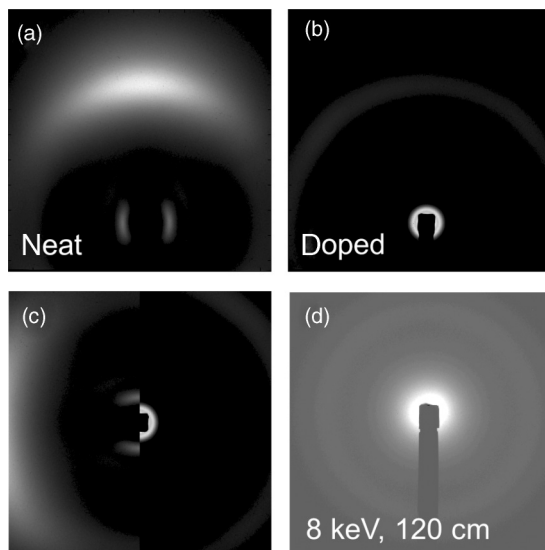


FIG. 1. (a) Two-dimensional x-ray diffraction patterns of the neat 5CB and (b) and (d) nanoparticle-doped 5CB recorded at a temperature of 28 °C. (a) and (b) WAXS patterns recorded at 12 keV photon energy and 26 cm sample or detector distance. (c) Juxtaposition of (a) and (b). (d) SAXS pattern of doped 5CB.

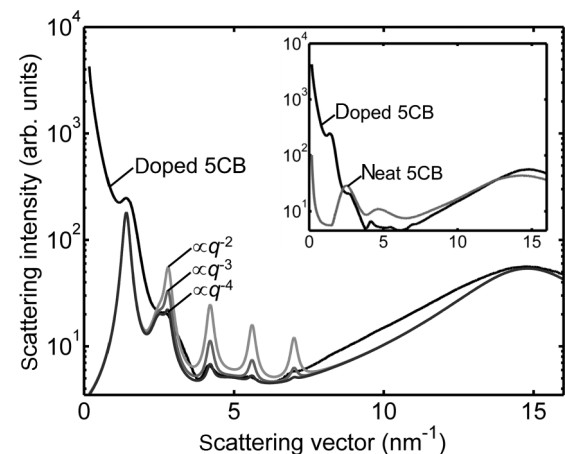


FIG. 2. Experimentally recorded scattering curve of nanoparticle-doped 5CB and three model curves with Bragg peak amplitudes proportional to  $q^{-2}$ ,  $q^{-3}$ , and  $q^{-4}$ , respectively. The inset shows the scattering curves of the nanoparticle-doped and neat 5CB in comparison. The shown scattering curves were recorded at a temperature of 28 °C. The data were acquired with x-ray photon energy of 8 and 12 keV and a sample or detector distance of 120 (SAXS region) and 26 cm (WAXS region), respectively. The two sets of data were then merged by matching at  $q = 1.5$  nm $^{-1}$ .

from two-dimensional scattering data. As already revealed by the scattering patterns, the scattering curve of the neat LC showed three peaks at approximately 2.5, 5.0, and 14.9 nm<sup>-1</sup>. The peak at ≈5 nm<sup>-1</sup> is a second order reflection of the peak at ≈2.5 nm<sup>-1</sup>. This peak corresponds to a  $d$  spacing of  $d_{\parallel} = 2\pi/2.5 \text{ nm}^{-1} = 2.5 \text{ nm}$ , the length of a 5CB dimer, as expected [15]. The peak observed at 14.8 nm<sup>-1</sup> corresponded to a spacing of  $d_{\perp} = 0.43 \text{ nm}$ , which was also reported in the literature [15]. In addition to these three peaks, some scattering is also observed in the region of  $q = 0.25\text{--}1.5 \text{ nm}^{-1}$ . Presumably, this small-angle scattering is caused by long range orientational order fluctuations in the neat LC. In the wide-angle region, the scattering curves of the neat and doped LCs both show a broad peak at  $q = 14.8 \text{ nm}^{-1}$ .

In contrast to the scattering curve of the neat LC, the scattering curve of the doped LC shows strong scattering in the range of  $q = 0.25$  to  $\approx 1.5 \text{ nm}^{-1}$  caused by the dopant. In the range of  $q > 1.4 \text{ nm}^{-1}$ , a Bragg signal at  $q \approx 1.4 \text{ nm}^{-1}$  and 4 higher orders of this reflection centered at  $q \approx 2.8, 4.2, 5.6,$  and  $7.0 \text{ nm}^{-1}$  can be identified in the scattering curve of the doped LC. These signals are apparently caused by a soft multilayered structure with a characteristic spacing of  $d_1 \approx 4.49 \text{ nm}$ . X-ray scattering of multilayered structures can be analyzed by means of the paracrystalline theory (reviewed in Ref. [21]) under the assumption that the radius of curvature of the multilayers is large compared to the thickness of the individual layers,

$$I(q) = \frac{S(q)|F(q)|^2}{q^2}. \quad (1)$$

In this model [Eq. (1)], the factor  $q^{-2}$  is the Lorentz correction for a nonoriented powder sample. The structure factor  $S(q)$  describes Bragg scattering due to the crystalline nature of the layered system. The factor  $F(q)$  is the form factor of the individual layers. In the paracrystalline theory, the form factor of a flat particle [22] is applied to describe the intensity variation in the Bragg peaks. The form factor of a flat particle (a layer) corresponds to the Fourier transform of the electron density distribution  $\eta(r)$  parallel to the layer normal,

$$F(q) = \int_{-d/2}^{d/2} \eta(r) \cos(qr) dr. \quad (2)$$

The form factor for multilayered structures describes a characteristic decay in intensity of the higher order Bragg peaks  $I_h$  proportional to  $q^{-2}$  [22]. Accordingly, in soft multilayered structures, the scattering intensity of the Bragg peaks  $I_h$  decays proportional to the peak intensity of the fundamental peak,

$$I_h = I_1/q^4. \quad (3)$$

The scattering curve of the doped LC was modeled with five Lorentzians centered at the positions of  $q = 1.4, 2.8, 4.2, 5.6,$  and  $7.0 \text{ nm}^{-1}$ . Three Lorentzians, centered at the peak positions of the neat LC (2.5, 5, and 14.8 nm<sup>-1</sup>), were also added. The two peaks at 2.5 and 5 nm<sup>-1</sup> account for the neat LC, which is also present in the doped sample. The third peak at 14.8 nm<sup>-1</sup> describes the Bragg reflection caused by  $d_{\perp}$ . Three different models are shown along with the experimental scattering curve of the doped LC (Fig. 2).

These models differ in the decay of the amplitudes of the five Lorentzians centered at the positions of  $q = 1.4, 2.8, 4.2, 5.6,$  and  $7.0 \text{ nm}^{-1}$ , which account for the Bragg scattering caused by the multilayer structure. The third model curve where the amplitudes of these five Lorentzians decay proportional to  $q^{-4}$  fits the data much better than the two model curves where the amplitudes decay proportional to  $q^{-2}$  and  $q^{-3}$ , respectively. Such a characteristic decay proportional to  $q^{-4}$  indicates a multilayered structure. Compared to the neat LC, the scattering intensity in the doped sample is higher in the range of  $q < 2.5 \text{ nm}^{-1}$  (Fig. 4, inset) due to scattering caused by the inorganic nanoparticles and due to the intense fundamental Bragg peak of the multilayer structure centered at  $q = 1.4 \text{ nm}^{-1}$ . According to the peak positions, the layer thickness of the individual layers corresponds to  $d_l \approx 4.49 \text{ nm}$ . Lorentzian peaks with a full width at half maximum (FWHM) =  $0.25 \text{ nm}^{-1}$  were used in the model curves for the five Lorentzians centered at  $q = 1.4, 2.8, 4.2, 5.6,$  and  $7.0 \text{ nm}^{-1}$ . An FWHM of  $0.25 \text{ nm}^{-1}$  corresponds to a correlation length of  $2\pi/0.25 \text{ nm}^{-1} \approx 25 \text{ nm}$  or a minimum thickness of five to six layers. In the fabrication step, oleic acid was added as a surfactant, and oleic acid was grafted onto the nanoparticles during the milling process. The characteristic molecular spacing of a single oleic acid molecule in the crystal is 2.03 nm [23] where oleic acid shows dimerization with a characteristic spacing of not more than 4.06 nm. Both the length of a single oleic acid molecule and the length of oleic acid dimers would not fit to the observed layer spacing. Oleic acid is not covalently bonded to the nanoparticles. In the heptane dispersion, oleic acid is adsorbed at the surface of the inorganic nanoparticles. The 5CB molecules possess a polar head group, may adsorb at the surface of the BaTiO<sub>3</sub> nanoparticles, and replace oleic acid molecules. Single oleic acid molecules as well as dimers may be solvated by 5CB. In the doped sample, 5CB is available even in excess concentrations. Most likely, 5CB molecules replace oleic acid at the nanoparticle surface. The present results indicate that 5CB dimers form a bilayer structure. A similar phenomenon where one to two crystalline layers were found to be present on a solid substrate in the SmA, nematic, and isotropic phases, was previously reported [24] for a simple calamitic mesogen. The thin crystalline layers were found to melt around 30 °C above the clearing point of this mesogen. In the nematic phase, 5CB molecules are well known to form dimers with a length of  $l_d \approx 2.5 \text{ nm}$ , which is smaller than the interlayer spacing of  $d_l \approx 4.49 \text{ nm}$ . In the crystal, 5CB molecules show both dipole-dipole interactions and London interactions. The unusual interlayer spacing of the soft multilayered structure may be explained by a model where two smectic layers of 5CB dimers (each stabilized by dipole-dipole interactions) possess additional stabilization by London interactions (Fig. 3). If so, the interlayer spacing  $d_l$  would be smaller than  $2l_d = 5 \text{ nm}$  as observed in the experiment ( $d_l \approx 4.49 \text{ nm} < 2l_d$ ). In order to proof the structure of the multilayers, a fit of the form factor of the layered structure with a model of the electron density distribution parallel to the layer normal  $\eta(r)$  would be desirable. However, in the present experiments, the remainder of neat LC in the doped LC prevents this type of analysis. In future studies of similar systems, the experimental procedure could be adjusted in order



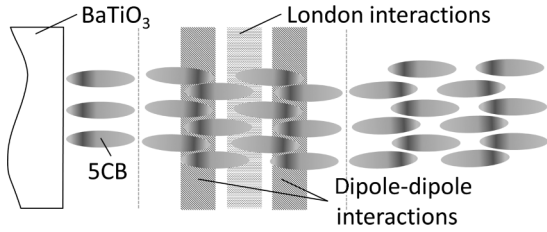


FIG. 3. Scheme of a multilayer of 5CB molecules with a high interlayer distance grafted onto the surface of a BaTiO<sub>3</sub> nanoparticle. The individual layers are stabilized by dipole-dipole interactions and London interactions.

to further purify the doped LC and to prevent remainders of the neat LC. Anyway, the present results show that the impact of milled BaTiO<sub>3</sub> nanoparticles on a simple calamitic mesogen, such as 5CB is highly nontrivial and leads to unusual molecular arrangements at the nanoparticle surface, which can contribute to the unusual behavior of nanoparticle-doped LC dispersions.

**B. Experiments varying temperature**

Small-angle x-ray scattering with a sample or detector distance of 120 cm and photon energy of 12 keV was conducted with doped 5CB. The low-angle limit of the present investigations was 0.1 nm<sup>-1</sup>. The scattering curves of the doped sample showed a characteristic shoulder at 1.42 nm<sup>-1</sup> (Fig. 4), presumably caused by a Bragg reflection of the multilayered structure described in Sec. III A. The scattering curve of the neat 5CB at 27 °C is shown for comparison. The samples were heated above 27 °C. The scattering intensity decreased with rising temperature. But the shoulder at 1.42 nm<sup>-1</sup> was preserved, which indicated a surprising high temperature stability of the multilayered structure. The multilayers were still present at 100 °C where heating was stopped. In the region of  $q < 1.4 \text{ nm}^{-1}$ , the dopant caused significant scattering. The scattering in this region was studied with the sample or detector distance of 120 cm and photon energy of 8 keV. Guinier plots [22] are shown in the

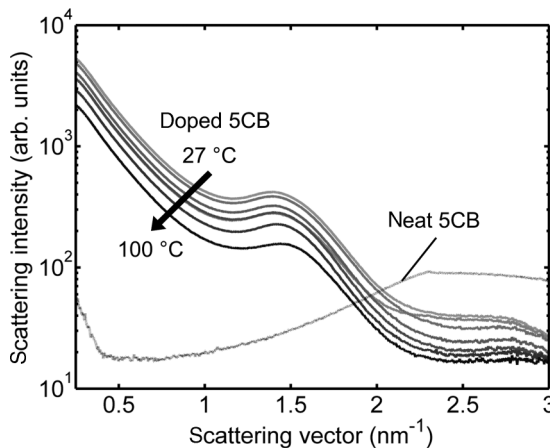


FIG. 4. Scattering curves of the doped 5CB (at 27 °C, 35 °C, 40 °C, 55 °C, 70 °C, 85 °C, and 100 °C) and the neat 5CB (at 27 °C) recorded with a 12 keV x-ray beam and a sample or detector distance of 120 cm.

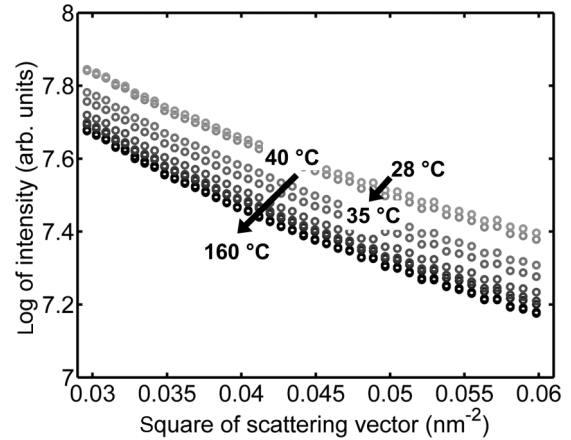


FIG. 5. Guinier plots of small-angle x-ray scattering data recorded for nanoparticle-doped 5CB at temperatures of 28 °C, 35 °C, 40 °C, 60 °C, 80 °C, 100 °C, 120 °C, and 160 °C.

$q$  range of 0.17–0.25 nm<sup>-1</sup> (Fig. 5). With rising temperature, the curves shift to lower intensity with a characteristic step between 35 °C and 40 °C where pure 5CB possesses the  $N \rightarrow I$  phase transition. Presumably, this step was caused by pure 5CB remaining in the solution. The slope of the straight lines fitted to the data is approximately temperature independent ( $s \approx 8.15 \text{ nm}^2$ ). The slope of the Guinier plots yields a radius of gyration  $R_g = (3s)^{0.5} = 4.95 \text{ nm}$  [22]. Although x-ray scattering in the region of  $0.1 \text{ nm}^{-1} < q < 1.4 \text{ nm}^{-1}$  was dominated by the dissolved inorganic nanoparticles, the form factor could not be extracted from the scattering curves because x-ray scattering from the LC made an additional contribution to x-ray scattering.

**IV. CONCLUSIONS**

In the present experiments, the liquid crystal 5CB was doped with a dispersion of milled BaTiO<sub>3</sub> nanoparticles. The growth of crystallites with a soft multilayer structure of 5CB molecules was observed. The multilayers possessed a coherence length of  $\approx 25 \text{ nm}$  at ambient temperature. A waxlike substance phase separated and segregated out of 5CB, which led to a large Bragg scattering with a decay in peak intensity proportional to  $q^{-4}$ , which was characteristic for soft multilayered structures. The scattering was observed at a temperature of 100 °C, which was more than 60 °C higher than the clearing temperature of the neat 5CB. It was not possible to quantitatively analyze the scattering curve and to extract the form factor of the multilayer structure in order to analyze the electron density distribution parallel to the layer normal. Anyway, a qualitative model of the scattering curve, based upon Lorentzian peaks, was presented, and the layer spacing of  $d_l = 4.49 \text{ nm}$  was extracted from the peak positions. The unusually high layer spacing was discussed, and a bilayer model was proposed where a bilayer of 5CB dimers (stabilized by dipole-dipole interactions) was stabilized by nonpolar interactions and was grafted onto the surface of the nanoparticles. The multilayer showed high temperature stability similar to a phenomenon reported in the literature for bilayers of another simple calamitic mesogen [24], which was deposited at a macroscopic solid surface. Further investigation is required in

order to understand the tendency of multilayer formation with the interlayer distance that cannot be explained by the smectic order of low symmetry. The results show an unusual assembly of a simple calamitic mesogen in a complex structure. The surface functionalized nanoparticles could easily be extracted and may be used as dopants for different LCs. In such systems, it will be interesting to see if the molecules of new LCs will undergo exchange with the adsorbed molecules as has been reported [25] in a different system for the surface of LC-test cells. For future experiments, it will be essential to further purify the samples. If so, a quantitative analysis of the scattering curve will be possible. It would be interesting to investigate different homologs of 4-*n*-alkyl-4'-cyanobiphenyl in order to test the influence of chain length and odd-even effects on the interlayer spacing of the presently reported multilayers

#### ACKNOWLEDGMENTS

The authors would like to thank V. Stanic and E. DiMasi (NSLS, Brookhaven National Laboratory) for their technical support and help in these experiments. Financial support by the German Research Foundation (Grants No. KI 411/14 and No. GRK 1464) and the European Science Foundation (EUROCORES, SONS II, "Self-organized nanostructures") is gratefully acknowledged. The participation of S.K. in this research was supported by the US Department of Energy, Office of Science, Basic Energy Sciences Grant No. DE-SC0001412. The use of the National Synchrotron Light Source, Brookhaven National Laboratory was supported by the US Department of Energy, Office of Science, Office of Basic Energy Sciences under Contract No. DE-AC02-98CH10886.

- 
- [1] M. Kreuzer, T. Tschudi, and R. Eidenschink, *Mol. Cryst. Liq. Cryst.* **223**, 219 (1992).
- [2] A. V. Glushchenko, G. Y. Guba, N. Y. Lopukhovich, V. M. Ogenko, V. Y. Reshetnyak, Y. A. Reznikov, and O. V. Yaroshchuk, *Mol. Cryst. Liq. Cryst.* **262**, 111 (1995).
- [3] H. Qui and T. Hegmann, *J. Mater. Chem.* **18**, 3288 (2008).
- [4] M. Urbanski, B. Kinkead, T. Hegmann, and H.-S. Kitzerow, *Liq. Cryst.* **37**, 1151 (2010).
- [5] G. L. Nealon, R. Greget, C. Dominguez, Z. T. Nagy, D. Guillon, J.-L. Gallani, and B. Donnio, *Beilstein J. Org. Chem.* **8**, 349 (2012).
- [6] M. Wojcik, W. Lewandowski, J. Matraszek, J. Mieczkowski, J. Borysiuk, D. Pocięcha, and E. Gorecka, *Angew. Chem., Int. Ed.* **48**, 5167 (2009).
- [7] O. Buchnev, A. Dyadyusha, M. Kaczmarek, V. Reshetnyak, and Y. Reznikov, *J. Opt. Soc. Am. B* **24**, 1512 (2007).
- [8] G. Cook, A. V. Glushchenko, V. Reshetnyak, A. T. Griffith, M. A. Saleh, and D. R. Evans, *Opt. Express* **16**, 4015 (2008).
- [9] A. Glushchenko, C. I. Cheon, J. West, F. Lic, E. Büyüktanir, Y. Reznikov, and A. Buchnev, *Mol. Cryst. Liq. Cryst.* **453**, 227 (2006).
- [10] F. Li, O. Buchnev, C. I. Cheon, A. Glushchenko, V. Reshetnyak, Y. Reznikov, T. J. Sluckin, and J. L. West, *Phys. Rev. Lett.* **97**, 147801 (2006).
- [11] G. Cook, V. Y. Reshetnyak, R. F. Ziolo, S. A. Basun, P. P. Banerjee, and D. R. Evans, *Opt. Express* **18**, 17339 (2010).
- [12] H. Atkuri, G. Cook, D. R. Evans, C.-I. Cheon, A. Glushchenko, V. Reshetnyak, Y. Reznikov, J. West, and K. Zhang, *J. Opt. A, Pure Appl. Opt.* **11**, 024006 (2009).
- [13] S. A. Basun, G. Cook, V. Y. Reshetnyak, A. V. Glushchenko, and D. R. Evans, *Phys. Rev. B* **84**, 024105 (2011).
- [14] G. Cook, J. L. Barnes, S. A. Basun, D. R. Evans, R. F. Ziolo, A. Ponce, V. Y. Reshetnyak, A. Glushchenko, and P. P. Banerjee, *J. Appl. Phys.* **108**, 064309 (2010).
- [15] A. J. Leadbetter and A. I. Mehtam, *Mol. Cryst. Liq. Cryst. Lett.* **72**, 51 (1981).
- [16] F. Vandenbrouck, S. Bardon, M. P. Valignat, and A. M. Cazabat, *Phys. Rev. Lett.* **81**, 610 (1998).
- [17] T. Sakai, K. Shirota, T. Yamada, H. Hoshi, K. Ishikawa, H. Takezoe, and A. Fukuda, *Jpn. J. Appl. Phys., Part 1* **35**, 3971 (1996).
- [18] T. Hanemann, W. Haase, I. Svoboda, and H. Fuess, *Liq. Cryst.* **19**, 699 (1995).
- [19] T. C. Huang, H. Toraya, T. N. Blanton, and Y. Wu, *J. Appl. Crystallogr.* **26**, 180 (1993).
- [20] S. Kumar, *Liquid Crystals* (Cambridge University Press, Cambridge, UK, 2001).
- [21] J. Lemmich, K. Mortensen, J. H. Ipsen, T. Hønger, R. Bauer, and O. G. Mouritsen, *Phys. Rev. E* **53**, 5169 (1996).
- [22] O. Glatter and O. Kratky, *Small Angle X-ray Scattering* (Academic, London, 1982).
- [23] S. Abrahamsson and I. Ryderstedt-Nähringbauer, *Acta Crystallogr.* **15**, 1261 (1962).
- [24] Y. Shi, B. Cull, and S. Kumar, *Phys. Rev. Lett.* **71**, 2773 (1993).
- [25] R. Guo, Y. Reznikov, K. Slyusarenko, and S. Kumar, *Appl. Phys. Lett.* **92**, 121911 (2008).